

Understanding the nature of atmospheric acid processing of mineral dusts in supplying bioavailable phosphorus to the oceans

Article

Published Version

Stockdale, A., Krom, M. D., Mortimer, R. J. G., Benning, L. G., Carslaw, K. S., Herbert, R., Shi, Z., Myriokefalitakis, S., Kanakidou, M. and Nenes, A. (2016) Understanding the nature of atmospheric acid processing of mineral dusts in supplying bioavailable phosphorus to the oceans. *Proceedings of the National Academy of Sciences of the United States of America*, 113 (51). pp. 14639-14644. ISSN 0027-8424 doi: <https://doi.org/10.1073/pnas.1608136113> Available at <https://centaur.reading.ac.uk/81675/>

It is advisable to refer to the publisher's version if you intend to cite from the work. See [Guidance on citing](#).

To link to this article DOI: <http://dx.doi.org/10.1073/pnas.1608136113>

Publisher: National Academy of Sciences

All outputs in CentAUR are protected by Intellectual Property Rights law, including copyright law. Copyright and IPR is retained by the creators or other copyright holders. Terms and conditions for use of this material are defined in

the [End User Agreement](#).

www.reading.ac.uk/centaur

CentAUR

Central Archive at the University of Reading

Reading's research outputs online

Understanding the nature of atmospheric acid processing of mineral dusts in supplying bioavailable phosphorus to the oceans

Anthony Stockdale^{a,1}, Michael D. Krom^{a,b}, Robert J. G. Mortimer^c, Liane G. Benning^{a,d}, Kenneth S. Carslaw^a, Ross J. Herbert^{a,2}, Zongbo Shi^e, Stelios Myriokefalitakis^f, Maria Kanakidou^f, and Athanasios Nenes^{g,h,i,j}

^aSchool of Earth and Environment, University of Leeds, Leeds LS2 9JT, United Kingdom; ^bDepartment of Marine Biology, Haifa University, Haifa 3498838, Israel; ^cSchool of Animal, Rural and Environmental Sciences, Nottingham Trent University, Brackenhurst Campus, Southwell, Nottinghamshire NG25 0QF, United Kingdom; ^dGerman Research Center for Geosciences, GFZ, 14473 Potsdam, Germany; ^eSchool of Geography and Earth Sciences, University of Birmingham, Birmingham B15 2TT, United Kingdom; ^fEnvironmental Chemical Processes Laboratory, Department of Chemistry, University of Crete, Heraklion, Greece, GR-71003; ^gSchool of Earth & Atmospheric Sciences, Georgia Institute of Technology, Atlanta, GA 30332; ^hSchool of Chemical & Biomolecular Engineering, Georgia Institute of Technology, Atlanta, GA 30332; ⁱInstitute for Environmental Research and Sustainable Development, National Observatory of Athens, Athens, Greece, GR-15236; and ^jInstitute of Chemical Engineering Sciences, Foundation for Research and Technology-Hellas, Patras, Greece, GR-26504

Edited by A. R. Ravishankara, Colorado State University, Fort Collins, CO, and approved November 4, 2016 (received for review May 29, 2016)

Acidification of airborne dust particles can dramatically increase the amount of bioavailable phosphorus (P) deposited on the surface ocean. Experiments were conducted to simulate atmospheric processes and determine the dissolution behavior of P compounds in dust and dust precursor soils. Acid dissolution occurs rapidly (seconds to minutes) and is controlled by the amount of H⁺ ions present. For H⁺ < 10⁻⁴ mol/g of dust, 1–10% of the total P is dissolved, largely as a result of dissolution of surface-bound forms. At H⁺ > 10⁻⁴ mol/g of dust, the amount of P (and calcium) released has a direct proportionality to the amount of H⁺ consumed until all inorganic P minerals are exhausted and the final pH remains acidic. Once dissolved, P will stay in solution due to slow precipitation kinetics. Dissolution of apatite-P (Ap-P), the major mineral phase in dust (79–96%), occurs whether calcium carbonate (calcite) is present or not, although the increase in dissolved P is greater if calcite is absent or if the particles are externally mixed. The system was modeled adequately as a simple mixture of Ap-P and calcite. P dissolves readily by acid processes in the atmosphere in contrast to iron, which dissolves more slowly and is subject to reprecipitation at cloud water pH. We show that acidification can increase bioavailable P deposition over large areas of the globe, and may explain much of the previously observed patterns of variability in leachable P in oceanic areas where primary productivity is limited by this nutrient (e.g., Mediterranean).

atmospheric processing | ocean macronutrients | desert dusts

Atmospheric inputs are an important source of externally supplied nutrients to the offshore ocean (1). Although all of the inorganic nitrogen (N) is water-soluble and immediately bioavailable, most phosphorus (P) and iron (Fe) are present as minerals that are not immediately soluble in water, hence not bioavailable (2, 3). Such mineral particles, if deposited to the surface ocean, may pass through the photic zone with no effect on primary productivity, owing to their high settling velocity and low solubility (2).

Atmospheric P can be important as the major external supply to the offshore ocean, particularly in oligotrophic areas of the open ocean (1) and areas that are P-limited, such as the Sargasso Sea (4) and Mediterranean (5). The most important source of atmospheric P is desert dust, which has been estimated to supply 83% (1.15 Tg·a⁻¹) of the total global sources of atmospheric P (6). Of that dust, it is estimated that 10% is leachable P. However, observations suggest that the fraction of leachable P in dust is highly variable (7–100%) (7). Only one global modeling study primitively simulates such variability, considering the reaction of protons with apatite minerals using a kinetic approach (8). The same study indicates that deposition of P from biological particles of terrestrial origin may be as important as leachable P from dust over the ocean in some regions and certain seasons. These recent findings translate to a large predictive uncertainty of

the bioavailable P input to the oceans. Studies show that although atmospheric N and Fe supply are of importance on a global scale, atmospheric P supply plays an important secondary role, especially through colimitation with either N or Fe (9, 10). The varying demands and resilience of different phytoplankton communities can have feedbacks on local limiting nutrients on relatively short time scales (11, 12). Additionally, evidence suggests feedbacks in the surface waters that may enhance the impact of the atmospheric supply of P (1, 13). This complex picture is yet to be replicated in global biogeochemistry models; therefore, it is not currently possible to put a limit on the importance of any atmospherically supplied P.

Previous studies have shown that atmospheric processes can increase Fe bioavailability in dust before being deposited to the ocean. Insoluble Fe, principally in the form of iron oxides, can be solubilized by interaction with acid gases that reduce the pH of atmospheric water to the level where solid phase Fe species can start to dissolve (14), by interaction with organic ligands, or by UV photoreduction (15). By contrast, the principal mineral species of P in aerosols, apatite minerals (e.g., hydroxyapatite [Ca₅OH(PO₄)₃]), are only expected to be solubilized by acid processes in the atmosphere, because they do not undergo photoreduction and

Significance

Mineral dust is the most important external source of phosphorus (P), a key nutrient controlling phytoplankton productivity and carbon uptake, to the offshore ocean. The bioavailable P in dust exhibits considerable and poorly understood variability. Detailed laboratory experiments elucidate and quantify the major processes controlling P dissolution in the atmosphere. Dust exposure to acids is the main driver of P mineral transformations, and a simple direct proportionality is found between the amount of bioavailable P dissolved from the dust and acid exposure. Simulations suggest that dust acidification increases leachable P over large areas of the globe and explains much of its variability in important oceanic areas where primary productivity is limited by this nutrient (e.g., North Central Atlantic, Mediterranean).

Author contributions: A.S., M.D.K., R.J.G.M., L.G.B., and K.S.C. designed research; A.S. and M.D.K. performed research; A.S., M.D.K., R.J.G.M., L.G.B., K.S.C., R.J.H., Z.S., S.M., M.K., and A.N. analyzed data; A.S., M.D.K., R.J.G.M., L.G.B., K.S.C., R.J.H., Z.S., and A.N. wrote the paper; and S.M., M.K., and A.N. developed the global modeling.

The authors declare no conflict of interest.

This article is a PNAS Direct Submission.

Freely available online through the PNAS open access option.

¹To whom correspondence should be addressed. Email: tony@biogeochemistry.org.uk.

²Present address: Department of Meteorology, University of Reading, Reading, RG6 6UA United Kingdom.

This article contains supporting information online at www.pnas.org/lookup/suppl/doi:10.1073/pnas.1608136113/-DCSupplemental.

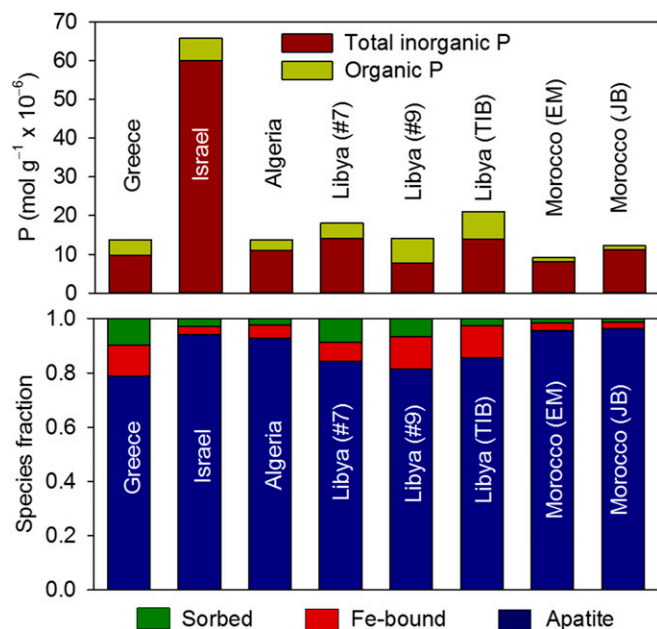


Fig. 1. P speciation in the dust and dust precursor samples, as determined by SEDEX. (Top) Concentrations of P present in the different samples. (Bottom) Relative fraction of the different inorganic P species.

calcium (Ca) is not strongly complexed by organic ligands. In a study on dust particles sampled in the eastern Mediterranean, Nenes et al. (7) found a correlation between increased leachable inorganic phosphorus (LIP) and increased acid exposure in the aerosol particles. Furthermore, the amounts of P released during acidification were consistent with the thermodynamic limit of solubility. However, no further insight on the mechanism and dissolution kinetics could be obtained.

The principal acid precursor species in the atmosphere are oxides of nitrogen and sulfur (NO_x and SO_x). These precursor species can be the result of natural processes, such as the oxidation of dimethyl sulfide released by phytoplankton in oceanic surface waters (16), volcanic eruptions (17), or lightning. However, at present, the main source of such gases in the northern hemisphere is anthropogenic (18). To a lesser degree, low-molecular-weight carboxylic acids (e.g., formic acid, acetic acid, oxalic acid) are generated in the atmosphere and can contribute acidity, especially in evaporated cloud droplets (18, 19).

Fresh and aged dust particles can be contained within cloud droplets that dissolve acidic gases but with pH levels that do not drop much below 4 (18). Although some cloud droplets condense to form rain, most cloud droplets evaporate to form wet aerosol particles. This process can result in a substantial drop in pH and an increase in ionic strength (IS) of the resultant film of water (20). This cycling between cloud droplets and wet aerosol particles can occur several times [an average of 10 cycles throughout the troposphere (18)] before the aerosol drops to earth by wet or dry deposition. Thus, the chemical conditions within and between clouds are very different, with relatively high pH and low IS in cloud droplets and low pH and high IS in wet aerosols (20–22). This cycling was investigated for its effect on Fe dissolution in the atmosphere by Shi et al. (23), who show that Fe is solubilized in wet aerosols and then reprecipitated as Fe nanoparticles in clouds. By contrast, the impact of pH changes or proton addition to atmospherically processed mineral dusts, and subsequent P dissolution, is virtually unknown.

This study sets out to investigate the nature, magnitude, and controls of atmospheric acid processes on the solubilization of mineral P in dust particles using samples collected during dust storms in Israel and Greece, as well as on dust precursors collected from surface soils in a variety of locations across the Sahara desert (map included in *SI Appendix*, Fig. S1.1). Experiments were

carried out using principally natural dust particles to mimic atmospherically relevant conditions, and thereby represent the amount of P solubilized by atmospheric acid processes. Results are interpreted by modeling the experimental systems using the geochemical PHREEQC (pH-redox-equilibrium calculation) model (24). Calculations using a global 3D atmospheric chemical transport model [Tracer Model 4 of the Environmental Chemical Processes Laboratory (TM4-ECPL)] (25) were used to estimate the potential global importance of these processes.

Results

Properties of Dusts. The highest P concentration was found in the dust sample from Israel (Fig. 1, Top). The sequential phosphate extractions (SEDEX) (26) revealed that apatite was the dominant P mineral (Fig. 1, Bottom). Total inorganic P [which includes leachable P, Fe-bound P, apatite P (Ap-P), and carbonate P] varied between 7.7 and 60.0 $\mu\text{mol}\cdot\text{g}^{-1}$, and represents 55–92% of the total SEDEX P in the sample. The remainder of the P was made up of organic P (full SEDEX data, mineral composition, and BET (Brunauer, Emmett, and Teller) surface area are provided in *SI Appendix*, section 3.1.2).

Effect of Protons and Fluid Volume on the Dissolution of Ca and P Minerals.

Fig. 2 shows the combined effects of pH and volume on the release of P from the Israel dust (legends used in this figure are used consistently in all subsequent figures and within *SI Appendix*). Both more acid pH values (at equal water volume) and higher volumes (at equal pH) yield greater P concentrations. The amount of P (Figs. 2 and 3) and Ca (Fig. 4) released from the dust was controlled by the amount of H^+ ions present and not the initial pH. Fig. 3 shows the released dissolved P plotted versus the protons in the experiments (as moles of H^+ per gram of dust). The data showed that below a critical proton concentration of ~ 0.1 mmol/g of dust [$-4 \log \text{mol}(\text{H}^+)/\text{g}$ of dust], the released P was only affected by water volume and not by the proton concentration. Above this proton concentration, an approximately linear increase in P with increasing initial proton concentration was seen, until a plateau was reached [approximately $-2.1 \log \text{mol}(\text{H}^+)/\text{g}$ of dust], where the acid-reactive mineral phosphate pool was exhausted. A similar pattern was seen with Ca (Fig. 4), although the critical proton concentration was slightly lower than seen for P. These figures indicate that above a given proton concentration, both Ca and P mineral phases are subject to dissolution. Fe was only above the detection limits in limited experiments where excess protons allowed the pH to remain low throughout the experiment. Results for the other dust samples yielded similar trends for all analytes (*SI Appendix*, section 3.2).

In all experiments the dust-solution mixtures tended to become buffered to neutral or alkali pH end points after 48 h of reaction.

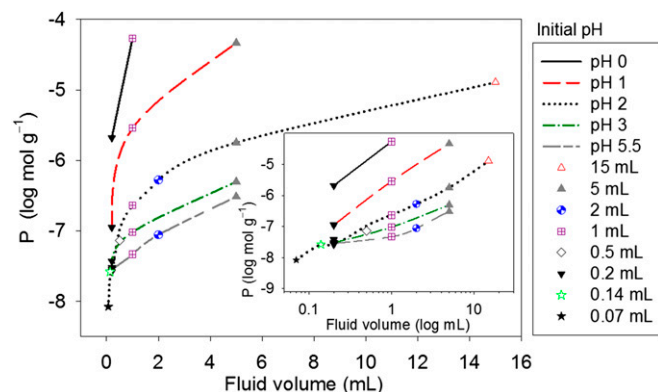


Fig. 2. Dissolved phosphate released from Israel dust in relation to pH and solution volume. Values are presented as moles per gram of dust. Dust masses were ~ 55 mg, and dust-to-volume ratios were 3.5–704.3 $\text{g}\cdot\text{L}^{-1}$. (Inset) Same data with the volume axis on a log scale.

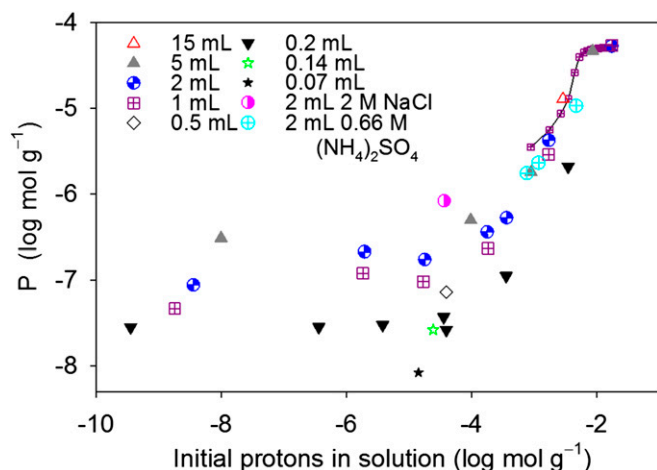


Fig. 3. Dissolved P (moles per gram of dust) released from Israel dust in relation to the absolute concentration of protons that were available for reaction at the start of the experiment. Dust masses were ~ 55 mg, and dust-to-volume ratios were 3.5–704.3 $\text{g}\cdot\text{L}^{-1}$. The crossed boxes connected by a solid line represent a sequential acid addition experiment (*SI Appendix*, section 2.1.3).

The exceptions were experiments where protons remained in excess and all Ca and P minerals were dissolved (*SI Appendix*, section 3.1.1 and Table S3.3). Even using buffered solutions (*SI Appendix*, section 3.1.1), the release profiles for P did not change from those release profiles described above. Similarly, instantaneous acid addition or slow acid diffusion also did not significantly alter the evolution of dissolved P in the experiments (*SI Appendix*, section 3.2.2). When we tested a sequential batch addition of acid, the results (Fig. 3, 1 mL experimental data connected by a solid line; also *SI Appendix*, section 3.2.3) were similar to experiments performed at higher total proton values through a single acid addition, implying consistent Ca and P mineral dissolution as the total proton exposure is increased. Finally, high IS also played a minimal role in driving P release (*SI Appendix*, section 3.2.3).

All experiments with the real dusts described above assumed that the reactive minerals (calcite and apatite) are found in every particle (“internally mixed”) at the ratio that can be calculated from the apatite and Ca concentrations determined in our study (*SI Appendix*, Table S3.1). Although dust particles may be “externally mixed” (particles of a given size have only calcite or apatite but not both), in reality the low-volume experiments brought the acidic fluid into contact with all particles, and thus the system behaved as internally mixed. Calcite (CaCO_3) controlled the H^+ content, and the released P was totally dependent on reactive mineral composition. These results were confirmed experimentally through analog dusts made up of single reactive mineral components (i.e., apatite only) or mixed reactive mineral components (apatite and calcite) that we used as dust proxies (*SI Appendix*, section 3.2.4). The analog experiments demonstrate that if dust particles were externally mixed, then there would have been more P released per H^+ amount compared with our real dust experiments (Figs. 2 and 3) because more protons are available for direct reaction with apatite.

Comparison of Experimental Results with Modeling. The close agreement between our precursor and real dust samples (*SI Appendix*, section 3.2.4) suggests that the interaction between calcite and apatite with acidity is the primary control of P solubility. This relationship is confirmed by thermodynamic calculations for a system containing only calcite, apatite, and solution (Fig. 5 and *SI Appendix*, section 3.3). Above $\sim 10^{-6}$ $\text{mol}\cdot\text{L}^{-1}$ for P and 10^{-4} $\text{mol}\cdot\text{L}^{-1}$ for Ca, there was agreement between measurements and predictions. Below these concentrations, predicted Ca and P deviated somewhat from the measurements, likely owing to desorption of loosely bound P (SEDEX sorbed pool; Fig. 1 and *SI Appendix*, Table S3.1) and Ca.

Discussion

We studied the dissolution of P-containing phases in the surface soils from areas that are known to be sources of Saharan dust (27), as well as two samples of dry deposited Saharan/Arabian dust. There was a relatively constant P speciation in the mineral composition of these dusts (Fig. 1). Given that the principal acid-soluble mineral, Ap-P, was, on average, $89 \pm 7\%$ of the total inorganic P and Fe bound-P was only $7 \pm 4\%$ of the acid-reactive mineral phases, we consider the proton reactions of only Ap-P and CaCO_3 as controlling the atmospheric conversion of mineral P to leachable forms. Other processes that affect the solubilization of Fe, such as photoreduction and organic complexation (12), are likely to have a minor role in increasing P bioavailability because only Fe bound-P will be affected by such processes. There is no evidence of organic P being affected by acidification. In addition to these acid-soluble phases, a small amount ($<7\%$) was in the sorbed inorganic-P pool (extracted by 1 M MgCl_2), which is likely to be solubilized directly into seawater (26).

Although our samples were collected or derived from widespread areas from the Sahara and Arabian deserts, they all had similar relative fractions of Ap-P, Fe-bound P, and adsorbed P. This finding is consistent with a common weathering regime across these deserts, which combines some chemical weathering, little plant growth to convert P minerals into plant biomass in situ, and often reprecipitation of CaCO_3 as caliche. However, we recognize that other regions of the Sahara, with different mineralogy [e.g., the Bodélé (28)], may exert an influence on the bulk properties of some Sahara dust plumes. Our samples had 7×10^{-4} to 3.3×10^{-3} $\text{mol}\cdot\text{g}^{-1}$ of acid-soluble Ca, which is 6–33% by mass of CaCO_3 . Although the P mineral speciation was similar between samples, there was considerable variability in the total P concentration (9.1×10^{-6} to 6.3×10^{-5} $\text{mol}\cdot\text{g}^{-1}$).

In the atmosphere, dust particles cycle between clouds, where they can become cloud condensation nuclei and wet aerosols. In clouds, there is a high water/dust ratio, low IS, and generally high pH, except in the unusual situation of very highly polluted air masses. Wet aerosols, which are generally formed when cloud water evaporates, contain a film of water and can have very low water/dust ratios, high IS, and low pH (23). Our experiments were designed to span these conditions within the practical limitations of laboratory handling. The key parameter in controlling the amount of P (and Ca) liberated from acid processing was the total amount of H^+ ions in the aqueous layer surrounding the dust particle and not the initial pH (Figs. 2–4). For all of our experiments, both CaCO_3 and Ap-P were rapidly dissolved (as measured by Ca^{2+} and orthophosphate liberated) and

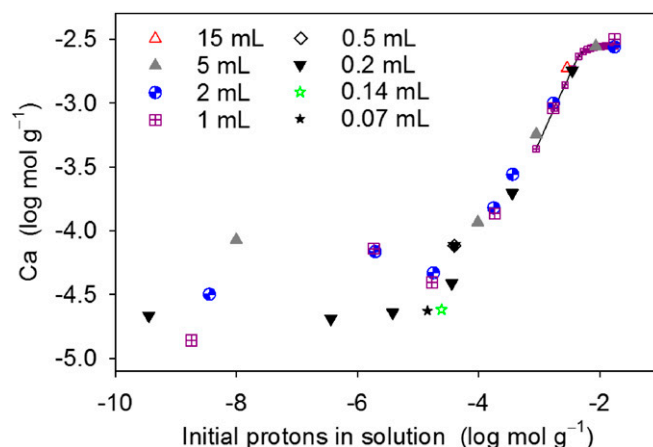


Fig. 4. Dissolved Ca (moles per gram of dust) released from Israel dust in relation to the absolute concentration of protons that were available for reaction at the start of the experiment. Dust masses were ~ 55 mg, and dust-to-volume ratios were 3.5–704.3 $\text{g}\cdot\text{L}^{-1}$.

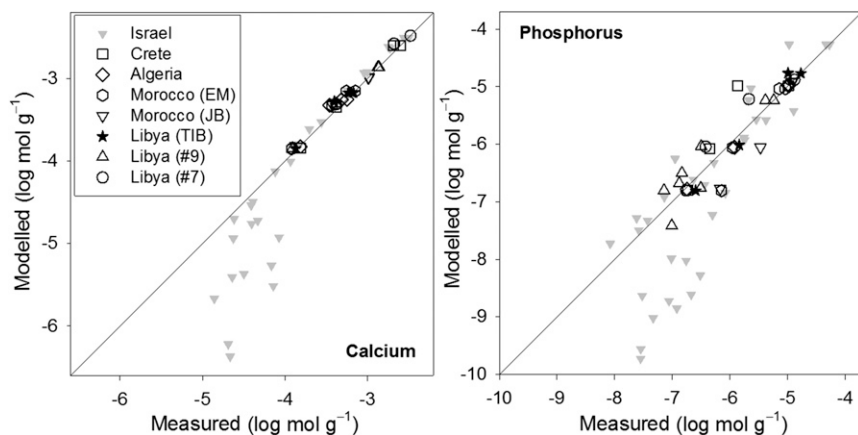


Fig. 5. Comparison of measured P and Ca dissolution from all dusts compared with equilibrium predictions made using PHREEQC.

H^+ ions were consumed on a time scale of seconds to minutes (*SI Appendix, section 3.1.1*). In most cases, the pH was controlled by rapid reaction with $CaCO_3$ to circumneutral values, as shown by the simple relationship between the decrease in H^+ ions being twice the increase in Ca^{2+} cations.

At low H^+ amounts ($<10^{-4}$ mol g^{-1} of dust), P was liberated over a wide range of H^+ ion concentrations. This result was interpreted as being due mainly to simple leaching of dissolved P from the samples into water, independent of the reaction of H^+ with acid-soluble minerals. This observation corresponds to the leachable P previously measured when dust was treated by deionized water or a very-low-strength leach (e.g., ref. 29). The amount of leached P is likely to be independent of whether there is $CaCO_3$ in the dust sample or not.

At proton concentrations above 10^{-4} mol of H^+ per gram of dust, there was a direct proportionality between P (and Ca) released and the amount of H^+ ions consumed (Figs. 2–4). This relatively simple pattern of P release continued until the level where all of the P minerals were exhausted. When the proton-reactive minerals were exhausted, the final solution pH was no longer circumneutral but remained acidic. The P released in experiments with the highest H^+ amounts corresponded approximately to the value of total inorganic P determined by SEDEX extraction. Similar trends were obtained for all of the other dust and dust precursor samples.

The relationship between P, Ca^{2+} , and H^+ ions for all of the test samples was confirmed by PHREEQC equilibrium modeling, in which there were similar increasing trends of P and Ca^{2+} obtained assuming a simple three-component model of calcite, hydroxyapatite, and H^+ ions. The model fit was better for Ca^{2+} (controlled by calcite and H^+ ions) than for P, where there was more scatter. This result is considered reasonable because there is more than one acid-soluble P mineral present in all of the natural samples, and the Ap-P is also likely to be made up from a number of different apatite minerals with different solubility behavior.

Our results also showed that increased IS caused slightly more dissolved phosphate to be liberated into solution. Where the major contributors to increased IS were ammonium and sulfate, the most common ionic species in aerosols (18), it was found that the amount of P released fits on the trend for the HCl-only data if the proton availability from the dissociation of ammonium ions (predicted from a final pH of 8) is allowed for. In our experiments using NaCl (IS = 2), which was used as a surrogate for evaporated sea salt, the liberated P increased by a factor of 4.3. In both cases, even if the IS decreases to that of rainwater, the dissolved P will remain in solution due to very slow precipitation kinetics and will be delivered as bioavailable P to the surface ocean (ref. 30 and references therein).

In the atmosphere, some mineral particles have both $CaCO_3$ and Ap-P on the same particle (internally mixed), whereas other particles have only one or the other mineral (externally mixed). Because acidity in the atmosphere is transferred to dust via the gas phase, the amount of dissolved P will vary between particles, depending on the amount of $CaCO_3$. There were no data available characterizing the degree of external mixing of $CaCO_3$ and Ap-P in

dust samples. However, we expect many of the particles to contain both $CaCO_3$ and Ap-P, because in many sedimentary rocks and desert soil systems, there is a close association between $CaCO_3$ and Ap-P. Both minerals precipitate in marine sediments during diagenesis (31), and such marine sediments are generally the source of Ap-P in desert soils (32). Furthermore, caliche forms in many desert soils, where Ca and bicarbonate produced by in-situ weathering are precipitated (33). However, our results show that in the situation where external mixing does occur, more P would be solubilized because on those particles with only Ap-P, there was no consumption of H^+ by $CaCO_3$ because it was absent from this experiment (*SI Appendix, section 3.2.4*). In reality, although we predict that many dust particles will be internally mixed, there will be a continuum and the balance between these two extremes may not be the same for all dust events.

Comparison with Fe Processes. The fraction of bioavailable Fe supplied to the ocean is also increased by acidic atmospheric processes (34). However, Fe dissolution is much slower than Ap-P (35). This behavior means that for internally mixed particles, essentially all of the H^+ ions will be neutralized by $CaCO_3$ before they react with Fe minerals. However, Fe-bearing particles are often externally mixed as clays (36) or Fe-rich particles (37). Thus, dissolution of Fe and P can happen simultaneously on different particles. Furthermore, Fe dissolution occurs principally in wet aerosols (low pH with high IS) (23). When the aerosol particles are activated into clouds at lower pH, the Fe is likely to reprecipitate as nanoparticles (38), whereas P does not reprecipitate. The only removal of P will be adsorption onto fresh Fe nanoparticles if both processes occur on the same particle/droplet. In that situation, both Fe and sorbed P are likely to be bioavailable.

The Potential Importance to the Global P Cycle and Supply to the Ocean. The main acids in the atmosphere, sulfuric and nitric acids, are generated by the oxidation of sulfur and N gases emitted by biogenic, volcanic, and anthropogenic sources (16–18), the latter of which is dominant at present. It has been noted that there is a higher fraction of LIP in polluted air masses (39, 40). Based on field samples collected in Crete, Nenes et al. (7) provided direct evidence of the increase in LIP in aerosols with increasing aerosol acidity. They suggest that this increased LIP is from polluted air masses from southern Europe bringing acid gases from the north to mix with the Saharan air mass. The increased fraction of LIP in atmospheric aerosols over the Bay of Bengal compared with atmospheric aerosols over the Arabian Sea has also been interpreted as due to the effect of acid processing of aerosols caused by anthropogenic activities (41). The action of the processes identified here may explain why aerosol samples across the North Central Atlantic can have greater fractions of soluble P than dust soil precursors or aerosols collected closer to the dust source (42). Our results demonstrate that atmospheric acid processes are extremely efficient in solubilizing P and provide further support to the finding by Nenes et al. (7) that acids can increase

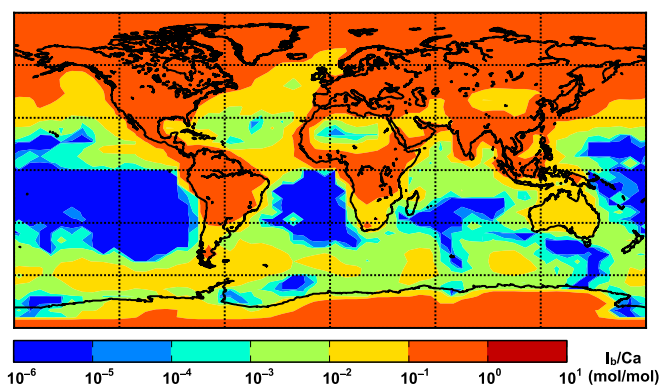


Fig. 6. Annual average ion balance over aerosol Ca. Calculations are performed with the global model framework of Myriokefalitakis et al. (25) using current-day aerosol emissions. Values of the ratio above 10^{-1} indicate regions where considerable solubilization of dust P is expected, where dust aerosol is present.

the delivery of bioavailable P from dust to the oceans. The amount of N fixation is also likely to increase because dust that has been acid-processed will contain increased amounts of both bioavailable P and Fe, which have been shown to limit N fixation (9).

To examine whether acid dissolution of dust P can be globally important, we simulate the acid exposure of dust and examine the extent to which it can occur. To do so, we quantify the ratio between dust Ca and its acid exposure. We quantify the ion balance, $I_b = 2[\text{SO}_4] + [\text{NO}_3] + [\text{Cl}] - 2[\text{Ca}] - [\text{NH}_4] - [\text{Na}] - 2[\text{Mg}] - [\text{K}]$ (where [X] represents the concentration of species X in the aerosol sample in moles per cubic meter of air) over aerosol Ca (Fig. 6; also *SI Appendix, section 3.4.*). Calculations are carried out with the global model framework of Myriokefalitakis et al. (25) using current-day aerosol emissions, and results are shown for the coarse fraction of dust and the model surface layer, which are representative of the dust that deposits to the surface. Values of the ratio above 10^{-1} indicate regions where considerable solubilization of dust P is expected. The simulations clearly indicate that the flux of bioavailable P over considerable regions of the ocean can be substantially increased by acidified dust. This increase is likely to be greater than the 0.59 Tmol of carbon per year that can be calculated from the bioavailable P predicted by the recent global modeling work that accounts for the kinetic Ap-P dissolution process (8).

In many locations, there has been a greater increase in N-containing gases, particularly NO_x and ammonia (NH_3), than in particulate P, which is transported in the atmosphere. The molar ratio is typically greater than 16:1 and often much larger. It has been reported that this supply tends to make surface waters more P-limited (29, 43). Our results suggest that this transformation is somewhat moderated by the relative increase in bioavailable P due to interaction between NO_x and dust particles. As a result, phytoplankton biomass and carbon uptake will increase even in areas of the ocean that are N-limited in the short term because P remains the element that causes a longer term increase in primary productivity (44). The implications of this added carbon export from anthropogenic pollution to ocean ecosystems has the potential to be widespread and considerable, affecting global primary productivity and the carbon cycle.

Methods

Dust and Precursor Dust Sources. Two dust samples and six size-fractionated dust precursor samples were used in this study (Table 1). The majority of the experiments were carried out with a dust sample deposited on a clean, flat surface during a dust storm in Rosh Pina, Israel (collected first in May 2012). A second dust sample was collected between June 1 and June 9, 2013, from a solar panel in Heraklion (Crete, Greece). Based on back-trajectory data from the HYSPLIT model (ready.arl.noaa.gov/HYSPLIT.php), the origins of these dust samples were the deserts of Saudi Arabia/Jordan/Iraq and North Africa, respectively. These two real dusts were used directly as collected, without size

fractionation or other preconditioning. In addition, six dust precursor samples collected from a variety of locations (mainly dry stream or lake bed soils) within the Sahara Desert (Table 1) were used to generate size-fractionated dusts using a dust tower separation and filtration methods (45). We used the $<10\text{-}\mu\text{m}$ fractions for our experiments, similar to previously used dust precursors that have been shown to be analogous to atmospherically sampled dust (45, 46). In this present study, the term “dust” is used to refer to both the dust precursor and the real dust samples unless otherwise stated.

Experimental Procedures.

SEDEX sequential P extraction. P speciation among the different operationally defined P pools was determined on 50–100 mg of each dust sample (Table 1) following the SPEXman SEDEX sequential extraction scheme (47), with the modification that step IIA for Fe-bound P followed the procedure of MacDonald (48). This modification removes the use of citrate, slightly alters the pH to 7.5, and increases the reaction time to 10 h. The absence of citrate means that the resulting solutions do not require any pretreatment, other than dilution, before analysis by the molybdate blue method (discussed below). Five P species were differentiated, namely: leachable or loosely sorbed; Fe-bound; a combined pool containing authigenic apatite, biogenic apatite, and CaCO_3 -bound; detrital apatite plus other inorganic P; and organic P. We defined apatite (Ap-P) as the combined phases extracted as diagenetic and detrital apatite, and CaCO_3 -bound P in the sequential SEDEX extraction scheme. Total inorganic P was defined as the sum of all of the phases except organic P. Methods for mineral composition and surface area analysis are in described in *SI Appendix, section 2.1.*

Phosphorous release experiments. The following experiments were performed on the dust samples using pH-adjusted but unbuffered solutions (HCl, Sigma-Aldrich; $\geq 37\%$ American Chemical Society reagent grade in 18.2 M Ω /cm of Milli-Q water) in an end-over-end stirrer for 48 h. Israel dust (55 ± 3 mg) was used as follows: pH 2 HCl with volumes of 70, 140, 210, and 500 μL and 1, 2, 5, and 15 mL; 0.2 mL of HCl at pH 0, 1, 2, 3, 4, and 5.5; 1 mL of HCl at pH 0, 1, 3, 4, and 5.5; 2 mL of HCl at pH 0.3, 1.3, 2.3, 3.3, 4.3, and 5.5; and 5 mL of HCl at pH 1, 3, and 5.5. Other dusts (30 ± 1 mg) were used at a volume of 1.2 mL at pH 0, 1, 1.8, and 2.4. Several initial experiments were carried out to determine the pH buffering capacities and the proton-dust reaction rates. We showed that almost all protons were consumed within ~ 200 s of starting the reaction and that the phosphate release was equally fast regardless of initial pH (*SI Appendix, sections 2.1.1 and 3.1.1*). Nevertheless, we performed the majority of our experiments over a conservative time period of 48 h, by which time all changes in concentration had been completed. At the end of these experiments, the mixture was passed through a 0.45- μm syringe filter (13-mm Whatman Puradisc polyethersulfone), and dissolved phosphate was determined as described below. In the experiments with solution volumes ≥ 2 mL, the final pH was measured following the 48-h exposures. The effect of high IS was tested by adding either ammonium sulfate or NaCl to reach $IS = 2$ (*SI Appendix, section 2.1.2*). Furthermore, additional experiments were carried out to evaluate the effect of sequential solution addition (*SI Appendix, section 2.1.3*), the effect of acid addition via dialysis (*SI Appendix, section 2.1.4*), and the behavior of simple laboratory-prepared dust analogs (*SI Appendix, section 2.1.5*).

Chemical Analysis of Supernatants. Dissolved inorganic P was analyzed using the molybdate blue reaction (49) after suitable dilution with matrix-matched standards on a segmented flow analyzer. For high concentrations (>50 nmol·L $^{-1}$), this analysis was done on a SEAL Analytical AA3. The relative standard deviation (RSD) was 2.2% ($n = 8$), and the limit of detection (LOD; $3 \times \text{SD}$ of blank) was 12 nmol·L $^{-1}$. Lower concentration samples were analyzed using a 100-cm WPI Liquid

Table 1. Samples used in this study and their source locations

Country of origin	Location	Coordinates
Dusts		
Greece	Crete	35°19'51"N, 25°40'04"E
Israel	Rosh Pina	32°58'12"N, 35°33'32"E
Precursor dusts		
Algeria	Bordj Mokhtar	21°19'30"N, 0°56'46"E
Morocco	El Miyit	30°21'53"N, 5°37'29"W
Morocco	Jebel Brahim	29°56'12"N, 5°37'43"W
Libya	7	32°02'42"N, 22°18'01"E
Libya	9	32°36'47"N, 22°11'42"E
Libya	Tibesti	25°35'N, 16°31'E

Locations are shown in the map included in *SI Appendix, Fig. S1.1*.

Waveguide Capillary Cell coupled to an Ocean Optics USB2000+ spectrophotometer with a precision ($n = 6$ of $60 \text{ nmol}\cdot\text{L}^{-1}$ samples) of 1.6% and a LOD of $2 \text{ nmol}\cdot\text{L}^{-1}$. Dissolved Ca and Fe concentrations in the supernatants were measured using a Thermo Scientific iCAP 7400 Radial inductively coupled plasma-optical emission spectrometer. The Ca and Fe detection limits were $<0.1 \text{ nmol}$ and $500 \text{ nmol}\cdot\text{L}^{-1}$, respectively, with RSDs of 1.5% and 1.8%, respectively [based on eight replicates of a $13 \text{ nmol}\cdot\text{L}^{-1}$ (Ca) or $9.0 \mu\text{mol}\cdot\text{L}^{-1}$ (Fe) standard]. Finally, pH was measured with a Mettler Toledo Seven Excellence meter coupled to an Inlab Expert Pro-ISM pH electrode calibrated with three National Institute of Standards and Technology traceable standard buffers (pH 4, pH 7, and pH 9.2; Mettler Toledo).

Geochemical Modeling of Experimental Systems. To evaluate the experimental results in terms of predicted equilibrium results, we used the geochemical modeling code PHREEQC (24), with the Lawrence Livermore National Laboratory database. Input conditions were based on the experimental starting solution conditions and assuming only hydroxyapatite and calcite were the reactive minerals present. The relative concentrations of these components were based on the dissolved Ca and P concentrations measured in the experiment for each dust under the most acid conditions.

1. Paytan A, McLaughlin K (2007) The oceanic phosphorus cycle. *Chem Rev* 107(2):563–576.
2. Eijssink LM, Krom MD, Herut B (2000) Speciation and burial flux of phosphorus in the surface sediments of the eastern Mediterranean. *Am J Sci* 300(6):483–503.
3. Shi Z, et al. (2012) Impacts on iron solubility in the mineral dust by processes in the source region and the atmosphere: A review. *Aeolian Res* 5:21–42.
4. Wu J, Sunda W, Boyle EA, Karl DM (2000) Phosphate depletion in the western North Atlantic Ocean. *Science* 289(5480):759–762.
5. Krom MD, Brenner N, Kress N, Gordon LI (1991) Phosphorus limitation of primary productivity in the eastern Mediterranean Sea. *Limnol Oceanogr* 36(3):424–432.
6. Mahowald N, et al. (2008) Global distribution of atmospheric phosphorus sources, concentrations and deposition rates and anthropogenic impacts. *Global Biogeochem Cy* 22(4):GB4026.
7. Nenes A, et al. (2011) Atmospheric acidification of mineral aerosols: A source of bioavailable phosphorus for the oceans. *Atmos Chem Phys* 11:6265–6272.
8. Myriokefalitakis S, Nenes A, Baker AR, Mihalopoulos N, Kanakidou M (June 8, 2016) Bioavailable atmospheric phosphorus supply to the global ocean: A 3-D global modelling study. *Biogeosci Discuss*, 10.5194/bg-2016-215.
9. Mills MM, Ridame C, Davey M, La Roche J, Geider RJ (2004) Iron and phosphorus co-limit nitrogen fixation in the eastern tropical North Atlantic. *Nature* 429(6989):292–294.
10. Moore CM, et al. (2008) Relative influence of nitrogen and phosphorus availability on phytoplankton physiology and productivity in the oligotrophic sub-tropical North Atlantic Ocean. *Limnol Oceanogr* 53:291–305.
11. Ward BA, Dutkiewicz S, Moore CM, Follows MJ (2013) Iron, phosphorus, and nitrogen supply ratios define the biogeography of nitrogen fixation. *Limnol Oceanogr* 58:2059–2075.
12. Moore CM, et al. (2013) Processes and patterns of oceanic nutrient limitation. *Nat Geosci* 6:701–710.
13. Van Mooy BAS, et al. (2009) Phytoplankton in the ocean use non-phosphorus lipids in response to phosphorus scarcity. *Nature* 458(7234):69–72.
14. Baker AR, Croot PL (2010) Atmospheric and marine controls on aerosol iron solubility in seawater. *Mar Chem* 120(1–4):4–13.
15. Spokes JL, Jickells TD, Lim B (1994) Solubilisation of aerosol trace metals by cloud processing: A laboratory study. *Geochim Cosmochim Acta* 58(15):3281–3287.
16. Liss PS, Hatton AD, Malin G, Nightingale PD, Turner SM (1997) Marine sulphur emissions. *Philos Trans R Soc Lond, B Biol Sci* 352:159–168.
17. Carbonnelle J, Dajčević D, Zettwoog P, Sabroux JC (1982) Gas output measurements from an active volcano. *Bull Volcanol* 45(3):267–268.
18. Seinfeld JH, Pandis SN (2006) *Atmospheric Chemistry and Physics: From Air Pollution to Climate Change* (Wiley, New York), 2nd Ed.
19. McNeill VF (2015) Aqueous organic chemistry in the atmosphere: Sources and chemical processing of organic aerosols. *Environ Sci Technol* 49(3):1237–1244.
20. Weber RJ, Guo H, Russell AG, Nenes A (2016) High aerosol acidity despite declining atmospheric sulfate concentrations over the past 15 years. *Nat Geosci* 9:282–285.
21. Meshkizde N, Chameides WL, Nenes A, Chen G (2003) Iron mobilization in mineral dust: Can anthropogenic SO_2 emissions affect ocean productivity? *Geophys Res Lett* 30(21):2085.
22. Zhu X, Prospero JM, Millero FJ, Savoie DL, Brass GW (1992) The solubility of ferric iron in marine mineral aerosol solutions at ambient relative humidities. *Mar Chem* 38(1–2):91–107.
23. Shi Z, Krom MD, Bonneville S, Benning LG (2015) Atmospheric processing outside clouds increases soluble iron in mineral dust. *Environ Sci Technol* 49(3):1472–1477.
24. Parkhurst DL, Appelo CAJ (2013) Description of input and examples for PHREEQC version 3—A computer program for speciation, batch-reaction, one-dimensional transport, and inverse geochemical calculations. *US Geological Survey Techniques and Methods* (Denver, CO) Book 6, Chapter A43. Available at pubs.usgs.gov/tm/06/a43/. Accessed May 4, 2015.
25. Myriokefalitakis S, et al. (2015) Changes in dissolved iron deposition to the oceans driven by human activity: A 3-D global modelling study. *Biogeosci* 12:3973–3992.
26. Ruttenberg K (1992) Development of a sequential extraction method for different forms of phosphorus in marine sediments. *Limnol Oceanogr* 37(7):1462–1482.

Global 3D Atmospheric Chemistry Transport Modeling Using TM4-ECPL. The ratio of $I_b \{2[\text{SO}_4] + [\text{NO}_3] + [\text{Cl}] - 2[\text{Ca}] - [\text{NH}_4] - [\text{Na}] - 2[\text{Mg}] - [\text{K}]\}$, where $[X]$ represents the concentration of species X in the aerosol sample (in moles per cubic meter of air) to Ca at the surface has been calculated using model TM4-ECPL (25), which takes into account anthropogenic and natural emissions as described in *SI Appendix, section 2.2.1*. and uses European Centre for Medium-Range Weather Forecasts Interim Reanalysis project (ERA-Interim) meteorology to drive atmospheric transport. The model uses the ISORROPIA (the Greek work for equilibrium) II thermodynamic model (50) to solve the $\text{K}^+ - \text{Ca}^{2+} - \text{Mg}^{2+} - \text{NH}_4^+ - \text{Na}^+ - \text{SO}_4^{2-} - \text{NO}_3^- - \text{Cl}^- - \text{H}_2\text{O}$ aerosol system and enables calculation of the aerosol water pH.

ACKNOWLEDGMENTS. We thank N. Mihalopoulos for fruitful discussions and for providing dust samples and N. Drake for providing dust precursor samples. Funding was provided by Grant RPG 406, entitled “Understanding the Delivery of P Nutrient to the Oceans,” from the Leverhulme Trust. Z.S. acknowledges support from the Natural Environment Research Council (NE/I021616/1). A.N. acknowledges support from a Cullen–Peck Fellowship and Georgia Power Scholar funds.

27. Ginoux P, Prospero JM, Gill TE, Hsu NC, Zhao M (2012) Global-scale attribution of anthropogenic and natural dust sources and their emission rates based on MODIS deep blue aerosol products. *Rev Geophys* 50(3):RG3005.
28. Hudson-Edwards K, Bristow CS, Cibin G, Mason G, Peacock CL (2014) Solid-phase phosphorus speciation in Saharan Bodélé Depression dusts and source sediments. *Chem Geol* 384:16–26.
29. Baker AR, Kelly SD, Biswas KF, Witt M, Jickells TD (2003) Atmospheric deposition of nutrients to the Atlantic Ocean. *Geophys Res Lett* 30(24):2296.
30. Golubev SV, Pokrovsky OS, Savenko VS (1999) Unseeded precipitation of calcium and magnesium phosphates from modified seawater solutions. *J Cryst Growth* 205(3):354–360.
31. Van Cappellen P, Berner RA (1991) Fluorapatite crystal growth from modified seawater solutions. *Geochim Cosmochim Acta* 55(5):1219–1234.
32. Gross A, et al. (2015) Variability in sources and concentrations of Saharan Dust over the Atlantic Ocean. *Environ Sci Technol Lett* 2(2):31–37.
33. Schlesinger WH (1985) The formation of caliche in soils of the Mojave Desert, California. *Geochim Cosmochim Acta* 49(1):57–66.
34. Meshkizde N, Chameides WL, Nenes A (2005) Dust and pollution: A recipe for enhanced ocean fertilization? *J Geophys Res* 110(D3):D03301.
35. Shi Z, et al. (2011) Influence of chemical weathering and aging of iron oxides on the potential iron solubility of Saharan dust during simulated atmospheric processing. *Global Biogeochemical Cycles* 25:GB2010.
36. Deboudt KA, Mussi GA, Flament P (2012) Red-ox speciation and mixing state of iron in individual African dust particles. *J Geophys Res* 117:D12307.
37. Kandler K, et al. (2009) Size distribution, mass concentration, chemical and mineralogical composition and derived optical parameters of the boundary layer aerosol at Tinfou, Morocco, during SAMUM 2006. *Tellus B Chem Phys Meteorol* 61(1):32–50.
38. Shi Z, et al. (2009) Formation of iron nanoparticles and increase in iron reactivity in mineral dust during simulated cloud processing. *Environ Sci Technol* 43(17):6592–6596.
39. Anderson LD, Faul KL, Paytan A (2010) Phosphorus associations in aerosols; what can they tell us about P bioavailability? *Mar Chem* 120(1–4):44–56.
40. Furutani H, Meguro A, Igushi H, Uematsu M (2010) Geographical distribution and sources of phosphorus aerosols over the North Pacific ocean. *Geophys Res Lett* 37:L03805.
41. Srinivas B, Sarin MM (2012) Atmospheric pathways of phosphorus to the Bay of Bengal: Contribution from anthropogenic sources and mineral dust. *Tellus B Chem Phys Meteorol* 64:17174.
42. Baker AR, Jickells TD, Witta M, Linge KL (2006) Trends in the solubility of iron, aluminium, manganese and phosphorus in aerosol collected over the Atlantic Ocean. *Mar Chem* 98:43–58.
43. Christodoulaki S, et al. (2016) Human-driven atmospheric deposition of N and P controls on the East Mediterranean marine ecosystem. *J Atmos Sci* 73(4):1611–1619.
44. Falkowski PG, Barber RT, Smetacek V (1998) Biogeochemical controls and feedbacks on ocean primary production. *Science* 281(5374):200–207.
45. Shi Z, et al. (2011) Iron dissolution kinetics of mineral dust at low pH during simulated atmospheric processing. *Atmos Chem Phys* 11(3):995–1007.
46. Lafon S, Sokolik IN, Rajot JL, Caquineau S, Gaudichet A (2006) Characterization of iron oxides in mineral dust aerosols: Implications for light absorption. *J Geophys Res* 111:D21207.
47. Ruttenberg KC, et al. (2009) Improved, high-throughput approach for phosphorus speciation in natural sediments via the SEDEX sequential extraction method. *Limnol Oceanogr Methods* 7:319–333.
48. MacDonald KR (2013) Evaluation of selective iron extraction techniques to quantify iron-bound phosphorus in sediments. Masters thesis (University of Hawaii, Honolulu).
49. Murphy J, Riley JP (1962) A modified single solution method for the determination of phosphate in natural waters. *Anal Chim Acta* 27:31–36.
50. Fountoukis C, Nenes A (2007) ISORROPIA II: A computationally efficient thermodynamic equilibrium model for $\text{K}^+ - \text{Ca}^{2+} - \text{Mg}^{2+} - \text{NH}_4^+ - \text{Na}^+ - \text{SO}_4^{2-} - \text{NO}_3^- - \text{Cl}^- - \text{H}_2\text{O}$ aerosols. *Atmos Chem Phys* 7(17):4639–4659.